Muon $g-2$ in Light of LHC and DM Experiments

Cem Salih Un,[1,2] Mario Gómez,[2] Qaisar Shafi,[3] and Amit Tiwari[3]

[1]*Department of Physics, Bursa Uludağ University, TR16059 Bursa, Turkey*

[2]*Departamento de Ciencias Integradas y Centro de Estudios Avanzados en Física Matemáticas y Computación, Campus del Carmen, Universidad de Huelva, Huelva 21071, Spain*

[3]*Department of Physics and Astronomy, University of Delaware, Newark, DE 19716, USA*

Abstract

We revisit and compare the muon $g-2$ implications of two classes of SUSY GUTs models in which the nonuniversal boundary conditions are imposed at $M_{\rm GUT}$. Even though the solutions to the muon $g-2$ discrepancy can be accommodated in both classes, the probe for such solutions at the current LHC and DM experiments can be challenging when the models are set up in a flavor-universal way. On the other hand, when the flavor nonuniversal models are considered, the implications for muon $g-2$ can be extended to a wider parameter space, and they can be probed through several experiments such as at LHC through the electroweakino productions or decay modes of the heavy Higgs bosons. They can yield interesting phenomenology to be tested in the DM experiments as well.

Keywords: supersymmetry, anomalous magnetic moment, collider, dark matter
DOI: 10.31526/LHEP.2023.360

1. INTRODUCTION

In this proceeding, we present some results about the implications of some classes of supersymmetric models for the muon anomalous magnetic moment (hereafter muon $g-2$) when nonminimal boundary conditions are imposed in the supersymmetric grand unified theories (SUSY GUTs) at the grand unification scale ($M_{\rm GUT}$). The results are based on our previous studies in [1–3]. After the recent update in the experimental measurements of muon $g-2$ by the Fermilab collaboration [4], combining its earlier measurements by the Brookhaven National Laboratory [5] results in a 4.2σ deviation from the Standard Model (SM) predictions [6], which can be expressed as follows:

$$\Delta a_\mu \equiv a_\mu^{\rm exp} - a_\mu^{\rm SM} = (25.1 \pm 5.1) \times 10^{-10}. \quad (1)$$

Despite all its success, it is very well known that the SM can form only an effective theory, and Supersymmetry (SUSY) is one of the compelling candidates for models beyond SM (BSM). The muon $g-2$ discrepancy given in equation (1) can be solved or ameliorated by the presence of new particles directly coupling to muons [7–12]. Accommodating a solution to the muon $g-2$ discrepancy consistent with several constraints in SUSY models usually requires relatively light sleptons, while the strongly interacting supersymmetric particles (squarks and gluino) are required to be heavy by the Higgs boson mass [13, 14] and the experimental results from the Large Hadron Collider (LHC) [15–21]. Even though a mass spectrum of heavy squarks and relatively lighter sleptons can be adjusted at the low-scale SUSY studies, this splitting between different sectors can yield a strong impact on SUSY GUTs. For instance, it is well known that the Higgs boson mass constraint yields a considerably heavy supersymmetric particles in minimally built GUT models [22–25]. Another tension can be realized with the recent mass bounds on the gluinos [15, 16], when one assumes the universal gaugino masses at $M_{\rm GUT}$.

Such tensions mentioned in the previous paragraph arise due to the minimal boundary conditions imposed at $M_{\rm GUT}$. However, it is possible to build SUSY GUTs with nonuniversal boundary conditions by assuming new flavor symmetries [26–33], supersymmetry breaking through vacuum expectation values (VEVs) of fields from nonsinglet representations of the GUT symmetry [34–43], and several sectors breaking SUSY [44–48]. Another path to impose nonuniversal boundary conditions is to consider a cascade of symmetry breaking which results in the SM gauge group passing through some intermediate symmetries such as $SU(4)_c \times SU(2)_L \times SU(2)_R$ (referred to Pati-Salam model) from $SO(10)$ breaking [49–51]. In $SO(10)$ breaking, if VEV is developed in the direction of 210_H representation of $SO(10)$, it also breaks the left-right (LR) symmetry, which induces another nonuniversality between the left-handed and right-handed matter sparticles [52].

In this proceeding, we compare two classes of SUSY GUT models with nonuniversal boundary conditions by the muon $g-2$ implications and discuss possible perspectives to test in the LHC and dark matter (DM) experiments. The SUSY contributions to muon $g-2$ happen through the neutralino-slepton and chargino-sneutrino loops. However, if one considers their contributions in the flavor basis, it can be seen that the main contributions can be realized when the Neutralino is formed mostly by Bino [53–55]. While the other flavors contribute minorly, their contributions can be significant when the particles running in the loops are strongly degenerate in mass. Both classes arise from $SO(10)$ SUSY GUTs. One class assumes $SO(10)$ breaking into the Pati-Salam gauge group in which the LR symmetry is broken as well [1, 2]. The second class assumes a flavor symmetry which splits the third family matter sparticles from the first two families. In addition, this class considers a nonsinglet F-term SUSY breaking which results in nonuniversal gaugino masses at $M_{\rm GUT}$ [3].

If one assumes one of the neutralinos is the lightest supersymmetric particle (LSP), then it can be considered also a compelling dark matter candidate. However, as the solution to the muon $g-2$ discrepancy requires light Bino, the LSP neutralino typically has a very large relic density to be a compatible DM candidate. In this case, one needs to identify coannihilation scenarios to reduce the relic density. In addition, muon $g-2$ fa-

vors light sleptons and charginos, and in this case, the LSP can coannihilate with the charginos and/or sleptons. If these coannohilation processes take part strongly, they can lead even to a very low relic density for the LSP neutralino. In this context, DM phenomenology provides one of the strongest constraints, and each kind of LSP can yield interesting dynamics and implications for direct and indirect DM detection experiments.

2. SUPERSYMMETRIC PATI-SALAM MODEL

In this section, we first consider a class of SUSY GUTs in which $SO(10)$ breaks into the Pati-Salam group. We assume a breaking mechanism in which the LR symmetry is also broken. In this case, the fundamental parameters of the model and their ranges employed in our scans can be summarized as follows:

$$\begin{aligned} 0 \leq m_L &\leq 5\,\text{TeV}, \\ 0 \leq M_{2L} &\leq 5\,\text{TeV}, \\ -3 \leq M_3 &\leq 5\,\text{TeV}, \\ -3 \leq A_0/m_L &\leq 3, \\ 1.2 \leq \tan\beta &\leq 60, \\ 0 \leq x_{LR} &\leq 3, \\ -3 \leq y_{LR} &\leq 3, \\ 0 \leq x_d &\leq 3, \\ -1 \leq x_u &\leq 2, \end{aligned} \tag{2}$$

where m_L denotes the mass of the left-handed matter sparticles, and M_2 and M_3 are the gaugino masses for the $SU(2)_L$ and $SU(3)_c$ gauge groups. A_0 is the universal trilinear term, which is varied by its ratio to m_L. Since the LR symmetry is broken, the Pati-Salam gauge group does not require $m_L = m_R$, $g_{2L} = g_{2R}$ and $M_{2L} = M_{2R}$, where g_{2L} and M_{2L} are the gauge coupling and gaugino mass for $SU(2)_L$, while g_{2R} and M_{2R} are the coupling and gaugino mass of $SU(2)_R$, and m_R denotes the mass terms for the right-handed matter sparticles. The LR breaking is controlled by the x_{LR} in the matter particles by defining the SUSY breaking masses as $m_R = x_{LR} m_L$. Similarly, y_{LR} measures the LR breaking in the gaugino sector as $M_{2R} = y_{LR} M_{2L}$. x_d and x_u parametrise the nonuniversality in the SSB masses of the MSSM Higgs fields at M_{GUT} as $m^2_{H_d} = x_d m^2_L$ and $m^2_{H_u} = x_u m^2_L$. Note that the fundamental parameters do not include M_1, the gaugino mass for $U(1)_Y$ group. $U(1)_Y$ is not an explicit part of the Pati-Salam group, but it is included implicitly as a superposition of the generators of $SU(4)_c$ and $SU(2)_R$, and M_1 is a dependent parameter which can be calculated as follows:

$$M_1 = \frac{3}{5} M_{2R} + \frac{2}{5} M_3. \tag{3}$$

Figure 1 displays the fundamental parameter space of the muon $g-2$ solutions with plots in the $\Delta a_\mu - m_L$, $\Delta a_\mu - m_R$, $\Delta a_\mu - M_1$, and $\Delta a_\mu - M_2$ planes. The top planes show that requiring the muon $g-2$ solution within 2σ bounds m_L at about 500 GeV from above, while its impact on m_R is relatively weaker, and one can accommodate muon $g-2$ solutions for $m_R \lesssim 1.5$ TeV. As expected, M_1 and M_2 are also bounded at about 1 TeV from above, as shown in the bottom planes.

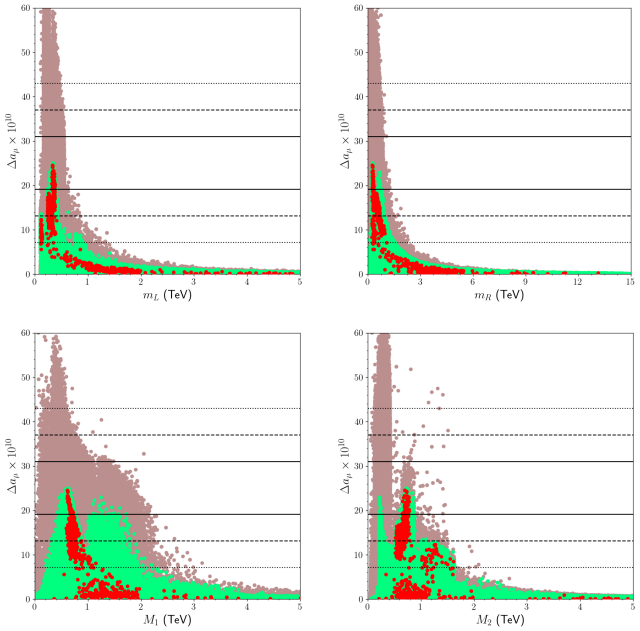

FIGURE 1: Plots in the $\Delta a_\mu - m_L$, $\Delta a_\mu - m_R$, $\Delta a_\mu - M_1$, and $\Delta a_\mu - M_2$ planes. All solutions are compatible with the REWSB and LSP neutralino conditions. The green points are allowed by the mass bounds and constraints from rare B-meson decays. The red points form a subset of green and they satisfy the Planck measurements on the relic density of LSP neutralino within 5σ. The horizontal solid, dashed, and dotted lines bound the regions which accommodate the muon $g-2$ resolution within 1σ, 2σ, and 3σ, respectively.

The SUSY contribution to muon $g-2$ is enhanced by the chirality flip between the sleptons running in a loop, and this enhancement is proportional to $\mu \tan\beta$ [53]. The $\Delta a_\mu - \mu$ plane in Figure 2 shows its effect as the SUSY contributions increase with large $\mu (\gtrsim 3.5\,\text{TeV})$. One would also expect large SUSY contributions when $\tan\beta$ is large, but the results in the $\Delta a_\mu - \tan\beta$ plane show that the LHC constraints (green) bounds $\tan\beta$ at about 20 from above, while the DM constraints (red) lower this bound at about 17. These bounds can be understood with the Higgs boson mass. As shown in the $\Delta a_\mu - m_h$ plane, even though large muon $g-2$ contributions can be realized, most of such solutions yield inconsistently light Higgs boson. Nevertheless, one can barely realize 125 GeV Higgs boson mass in the spectrum for the muon $g-2$ solutions within 2σ range of its experimental measurements. Since the muon $g-2$ solutions require light m_L and m_R, the third family sparticles cannot be heavy enough to lead to correct Higgs boson mass, since this class of models has flavor universal boundary conditions. In this case, the correct Higgs boson can still be realized when the mixing in the third family is maximal, which can be expressed as $X_t \simeq 2M_{\text{SUSY}}$ [56], where $X_t = A_t - \mu\cot\beta$ and $M_{\text{SUSY}} = \sqrt{m_{\tilde{t}_1} m_{\tilde{t}_2}}$. However, in this class of models, the largest muon $g-2$ contributions can be observed when $X_t \sim M_{\text{SUSY}}$ as seen from the $\Delta a_\mu - X_t/M_{\text{SUSY}}$ plane, and thus, the loop contributions to the Higgs boson mass cannot be enough, unless the suppression from $\tan\beta$ is ameliorated, which can happen with relatively lower $\tan\beta$ values.

We display the masses of stau and chargino in correlation with the LSP neutralino in Figure 3. As seen from the $m_{\tilde{\chi}^0_1} - m_{\tilde{\tau}_1}$

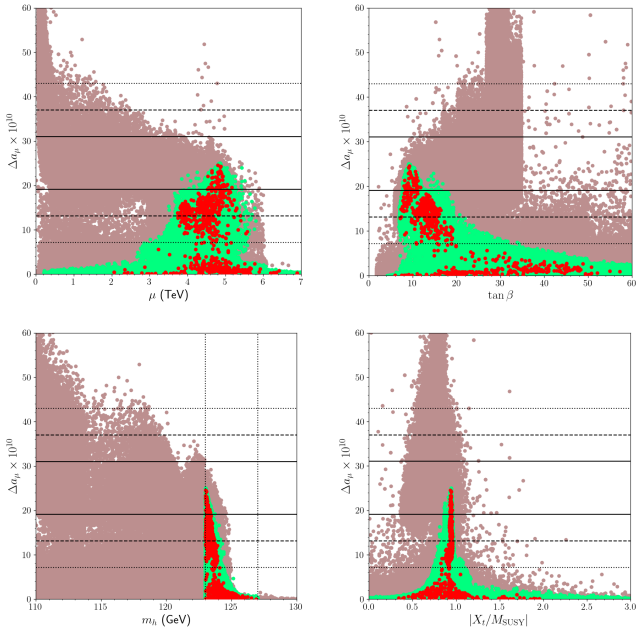

FIGURE 2: Plots in the $\Delta a_\mu - \mu$, $\Delta a_\mu - \tan\beta$, $\Delta a_\mu - m_h$, and $\Delta a_\mu - X_t/M_{\rm SUSY}$ planes. The meanings of colors and horizontal lines are the same as in Figure 1.

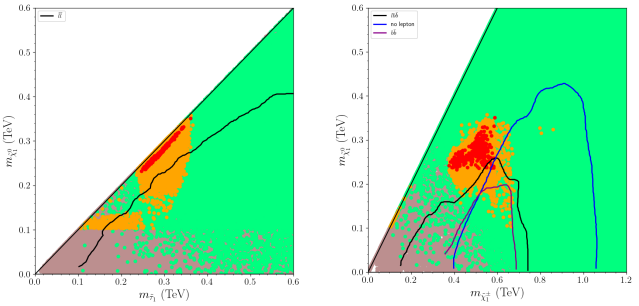

FIGURE 3: The Stau (left) and chargino (right) in correlation with the LSP neutralino mass. All points are compatible with the REWSB and LSP neutralino conditions. Green points are allowed by the mass bounds and constraints from rare B-meson decays. The orange points form a subset of green, and they accommodate the resolution to the muon $g-2$ discrepancy within 2σ. The red points as a subset of orange, additionally, yield the correct relic density of the LSP neutralino measured by the Planck satellite within 5σ uncertainty. The black curve in the $m_{\tilde\chi_1^0} - m_{\tilde\tau_1}$ plane displays the exclusion for the slepton masses with respect to the LSP neutralino masses from the analyses of the slepton pair production processes [57]. Similarly, the curves in the $m_{\tilde\chi_1^0} - m_{\tilde\chi_1^\pm}$ represent the exclusion curves from several LHC analyses over the chargino-neutralino production [58–60].

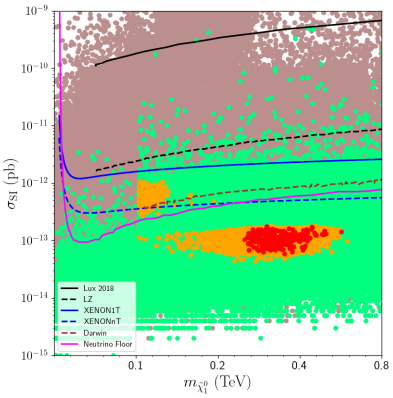

FIGURE 4: The spin-independent scattering cross-section of DM in correlation with its mass. The color coding is the same as in Figure 3. The solid (dashed) curves show the current (projected) results from LUX, LZ [61], XENON [62], and DARWIN [63] experiments for the spin-independent scattering cross-sections, whose color convention is given in the legend. The magenta curve represents the neutrino floor [64].

plane, the muon $g-2$ solutions (orange) can be accommodated when the stau is as heavy as about 350 GeV. However, some of these solutions can be excluded by the LHC analyses (below the black curve). On the other hand, if one requires the correct relic density for the LSP neutralino (red), such solutions can be realized only when the stau is nearly degenerate with the LSP neutralino (solutions around the black diagonal line). In this case, the stau and LSP neutralino form a compressed mass spectrum and they are allowed by the LHC constraints. On the other hand, chargino is allowed to be as heavy as about 600 GeV by the muon $g-2$ solutions, and the Planck measurements on the relic density of LSP neutralino bounds the chargino mass as $260 \lesssim m_{\tilde\chi_1^\pm} \lesssim 500$ GeV (red points). Even though the LHC analyses can exclude a significant portion of muon $g-2$ solutions, the most of the DM solutions are still allowed, and they can be tested during the Run-3 phase of LHC experiments.

As seen in Figure 3, the chargino and LSP neutralino masses are not very degenerate. Such a mass configuration typically indicates that the LSP neutralino is formed mostly by Bino. As mentioned before, the relic density of Bino is usually large, but it can be reduced through the coannihilation processes, and this class of models leads to stau-neutralino coannihilation to yield the correct relic density of the LSP neutralino. However, another challenge about the Bino-like LSP is typically low scattering cross-section at nuclei. As shown in Figure 4, its scattering cross-section is mostly of order 10^{-13} pb, which is way below the current probes and future projections of the direct detection experiments denoted by the solid and dashed curves. Nevertheless, these solutions lie below the neutrino floor (magenta curve). Therefore, testing such solutions in direct DM detection experiments requires more statistics and higher sensitivity, since the main background is formed by the neutrinos. We also observed some solutions which yield a relatively larger scattering cross-section (orange points at about 10^{-12} pb). Even though these solutions seem to be testable, they predict relic density of LSP neutralino lower than the Planck bound, and they cannot be accounted for the whole experimental observations. On the other hand, these solutions can be embedded into a larger model which proposes a multiple-component DM.

3. SPLIT FAMILIES AND NONUNIVERSAL GAUGINOS

Even though the family universal models can accommodate muon $g-2$ solutions despite the tensions with the Higgs boson mass, such solutions are not very easy to be tested at the

LHC and/or direct DM detection experiments, as discussed in the previous section. The Higgs boson mass constraints exclude all the large $\tan\beta$ solutions, which significantly suppresses the SUSY contributions to muon $g-2$. On the other hand, this tension arise from the family universal boundary conditions, and if the third family matter sparticles can have different masses than the first two family sparticles, the Higgs boson mass becomes almost completely independent of the SUSY contributions to muon $g-2$. In the second class of SUSY GUTs models, we assume the presence of a flavor symmetry at $M_{\rm GUT}$, which distinguishes the third family from the other families, and lead to a SUSY breaking in which the third family acquires independent SUSY breaking mass. The fundamental parameters and their ranges in our scan can be summarized as follows:

$$\begin{aligned} 0 \leq m_{0_{1,2}}, m_{0_3} \leq 5\,\text{TeV}, \\ 0 \leq M_1, M_2 \leq 2\,\text{TeV}, \\ -5 \leq M_3 \leq 5\,\text{TeV}, \\ -3 \leq A_0/m_{0_3} \leq 3, \\ 1.2 \leq \tan\beta \leq 60, \\ 0 \leq m_{H_d}, m_{H_u} \leq 5\,\text{TeV}, \end{aligned} \tag{4}$$

where the definitions of the parameters are the same as those in the previous section; however, in this case, the mass terms for the families are split in a way that $m_{0_{1,2}}$ denotes the SUSY breaking mass term for the first two families, while m_{0_3} is assigned for the mass term of the third family sparticles at $M_{\rm GUT}$.

Figure 5 displays the muon $g-2$ results in correlation with the GUT scale masses. As is observed in the previous class of models, the muon $g-2$ solutions mostly restrict the masses of the first two family sparticles. The $\Delta a_\mu - m_{0_{1,2}}$ plane shows that the muon $g-2$ solutions can be accommodated in a region where $m_{1,2} \lesssim 1\,\text{TeV}$. On the other hand, m_3 receives no impact from the muon $g-2$ condition, and it can be as heavy as about 4 TeV. Similarly, the gaugino masses can also exceed the TeV scale while the solution to the muon $g-2$ problem can be maintained.

Such heavy third family sparticles also improve the Higgs boson mass and remove the tension between the muon $g-2$ and the Higgs boson mass constraint, whose effect can be observed in the $\Delta a_\mu - \tan\beta$ plane. In contrast to the flavor universal models, the large $\tan\beta$ region is widely available, and indeed, the muon $g-2$ solutions favor this region better than the lower $\tan\beta$ region. As discussed in the previous section, μ also directly enhances the SUSY contributions to muon $g-2$ through the chirality flip between the sleptons running in the loops.

Observing a wider parameter space in the flavor nonuniversal framework also yields a richer DM phenomenology. Even though the Wino can be light, most of the muon $g-2$ solutions favor Bino-like LSP, and the light sleptons favored by the muon $g-2$ solutions also take part in slepton-neutralino coannihilation processes to reduce the relic density of Bino-like neutralino LSP. The top planes in Figure 7 show that smuon and stau can be nearly degenerate with the LSP neutralino in the mass scales from about 200 GeV to 550 GeV, and the solutions in this region can be identified as slepton-neutralino coannihilations. Similarly, when the chargino mass is between 300 and 600 GeV, it can be degenerate with the LSP mass and these solutions satisfy the Planck bound on the relic density of LSP

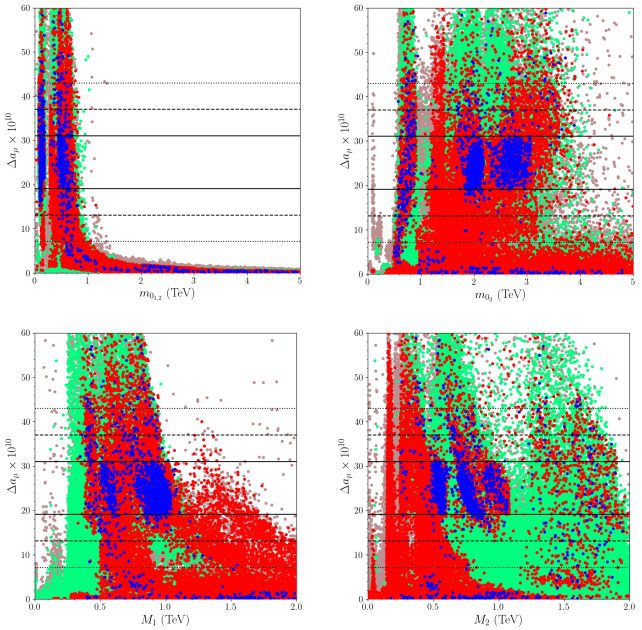

FIGURE 5: Plots in the $\Delta a_\mu - m_{0_{1,2}}$, $\Delta a_\mu - m_{0_3}$, $\Delta a_\mu - M_1$, and $\Delta a_\mu - M_2$ planes. All points are compatible with the REWSB and LSP neutralino conditions. Green points satisfy the mass bounds and the constraints from rare B-meson decays. Blue and red points form subsets of green. The solutions consistent with the Planck bound within 5σ uncertainty are shown in blue, while those yielding low relic density are represented in red. The solid, dashed, and horizontal lines show the regions which resolve the muon $g-2$ anomaly within the 1σ, 2σ, and 3σ intervals.

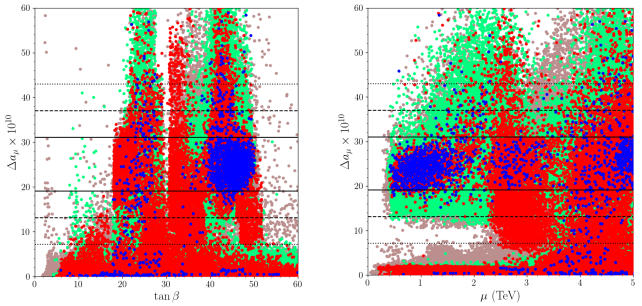

FIGURE 6: Plots in the $\Delta a_\mu - \tan\beta$ and $\Delta a_\mu - \mu$ planes. The color coding is the same as in Figure 5.

through the chargino-neutralino coannihilation. There are also solutions in which the chargino is very degenerate with the LSP in mass when its mass is between about 100 and 600 GeV (red solutions). These solutions represent the typical mass spectrum when the LSP neutralino is formed mostly by Wino; however, the chargino-neutralino coannihilation processes significantly reduce the relic density, and thus, these solutions lead to a very low relic abundance of LSP neutralino. Even though these solutions are excluded by the Planck bound, they can be embedded in larger models which propose multiple DM candidates. Finally, we also identify A-resonance solutions with $m_A \simeq 2m_{\tilde{\chi}_1^0}$ shown in the $m_A - m_{\tilde{\chi}_1^0}$ plane. These solutions can be realized when $m_A \in$ 900–1200 GeV.

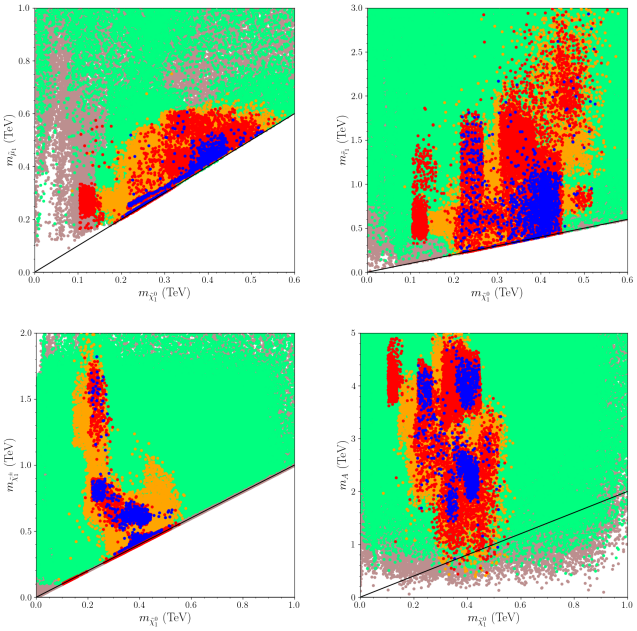

FIGURE 7: Plots in the $m_{\tilde{\mu}_1} - m_{\tilde{\chi}_1^0}$, $m_{\tilde{\tau}_1} - m_{\tilde{\chi}_1^0}$, $m_{\tilde{\chi}_1^\pm} - m_{\tilde{\chi}_1^0}$, and $m_A - m_{\tilde{\chi}_1^0}$ planes. All points are compatible with the REWSB and LSP neutralino conditions. Green points satisfy the mass bounds and constraints from rare B-meson decays. Orange points form a subset and they provide a solution to the muon $g-2$ discrepancy within 1σ. Red and blue points form subsets of orange. The solutions leading to a relic density for the LSP neutralino consistent with the Planck bound within 5σ are shown in blue, and those with low relic density are represented in red. The diagonal lines in the top and bottom-left plane indicate the mass degeneracy between the plotted particles, while in the bottom-right plane the diagonal line represents the resonance solution ($m_A = 2m_{\tilde{\chi}_1^0}$).

The variety in the coannihilation and annihilation solutions also yield different phenomenology which can be probed in the direct DM detection experiments. As shown in Figure 8, several orders of the scattering cross-section can be realized. The solutions yielding a large scattering cross-section usually predicts Wino-like LSP neutralino, and their scattering cross-section can be realized in a range from 10^{-12} pb to 10^{-10} pb. Even though some of those solutions can be excluded by the XENON1T experiment, some solutions with $\sigma_{\rm SI} \lesssim 10^{-12}$ pb will potentially be tested soon. There are also solutions with lower scattering cross-sections ($\sigma_{\rm SI} \lesssim 10^{-13}$ pb), which can also be expected to be tested in near-future direct detection experiments.

We exemplify our findings in the flavor nonuniversal framework with several benchmark points listed in Table 1. As one can see from their spectra, the first two family sleptons cannot weigh more than 500 GeV, and such mass scales for these sleptons can receive some impacts from LHC analyses during its Run-3 phase experiments. These solutions can be tested through the chargino-neutralino production which successively involves decays into the light sleptons and LSP neutralinos. The relevant SM backgrounds for this signal process include $\bar{t}t$ and WW, WZ, and ZZ-pair production; however, comparing their strengths in collisions [65–69], the main background is formed by top-pair production in which the

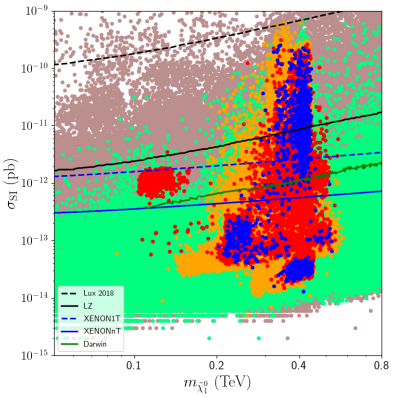

FIGURE 8: The spin-independent scattering cross-section of DM in correlation with its mass. The color coding is the same as in Figure 3. The solid (dashed) curves show the current (projected) results from LUX, LZ [61], XENON [62], and DARWIN [63] experiments for the spin-independent scattering cross-sections, whose color convention is given in the legend.

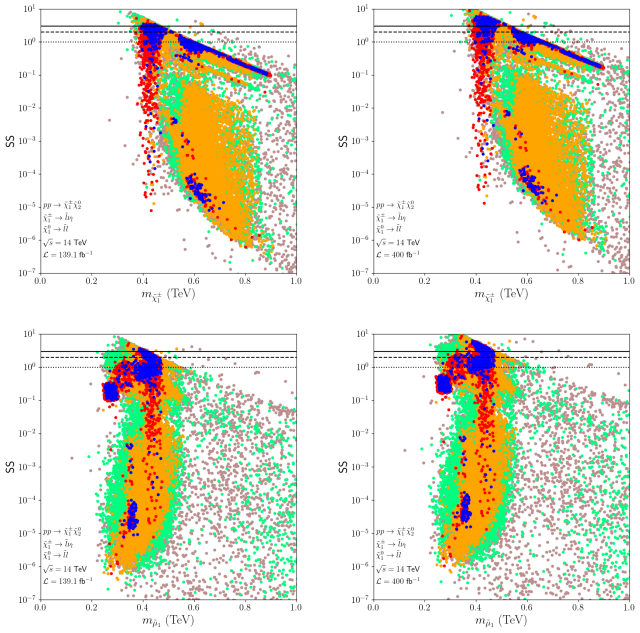

FIGURE 9: The expected probe on the chargino and slepton masses during the LHC-Run3 experiments. SS is the signal strength over the relevant background processes and plotted in correlation with the chargino (top) and slepton (bottom) masses for 139.1 fb^{-1} (left) and 400 fb^{-1} (right) luminosities. The color coding is the same as in Figure 7. The dotted, dashed, and solid horizontal lines correspond to SS $= 1, 2, 3$, respectively.

top quarks decay into W-bosons and the final state is formed by multiple leptons. Figure 9 shows the signal strength over the top-quark pair production in correlation with the masses of the chargino and sleptons. The currently integrated luminosity of LHC is 139.1 fb^{-1}, and the charginos can already be probed up to about 600 GeV (top-left). The targeted luminosity at the end of Run-3 phase is 400 fb^{-1}, and we observe that the Run-3 experiments can improve this bound as $m_{\tilde{\chi}_1^0} \gtrsim 700$ GeV (top-right). Similarly, the sleptons can be probed up to about 350 GeV currently, and one can expect them to be tested up

	Point 1	Point 2	Point 3	Point 4	Point 5	Point 6
$m_{0_{1,2}}$	325	112.3	160.3	499.5	444.7	120.7
m_{0_3}	1989	2166	2000	3025	2472	1893
M_1	854.8	1010	817.8	885	1073	977.9
M_2	483.4	759.4	721.1	523	514	745.6
M_3	2139	2079	1764	2691	−3891	1956
A_0/m_{0_3}	−3.0	−2.0	−2.2	−2.7	−1.4	−1.3
$\tan\beta$	20.2	44.9	43.5	43.3	44.4	47.8
μ	4508	1861	1537	5039	4080	468.9
$\Delta a_\mu \times 10^{10}$	24.6	25.6	28.9	26.1	24.3	22.3
m_h	125.6	124.4	124.4	125.6	123.1	123.4
m_H	3963	2540	2255	4148	946.8	2062
m_A	3964	2540	2255	4148	946.8	2062
$m_{H^\pm}$	3967	2542	2258	4150	951.1	2065
$m_{\tilde{\chi}_1^0}, m_{\tilde{\chi}_2^0}$	365.2, 387	433.1, 617.7	348.8, 587.4	380.6, 419.9	513.7, 540.5	411.2, 562.8
$m_{\tilde{\chi}_3^0}, m_{\tilde{\chi}_4^0}$	4495, 4495	1909, 1911	1576, 1578	5028, 5029	4160, 4160	639.2, 682
$m_{\tilde{\chi}_1^\pm}, m_{\tilde{\chi}_2^\pm}$	387.2, 4496	617.9, 1912	587.6, 1579	420.1, 5029	540.7, 4160	561.5, 680.8
$m_{\tilde{g}}$	4470	4344	3724	5560	7841	4108
$m_{\tilde{u}_1}, m_{\tilde{u}_2}$	3843, 3849	3719, 3740	3202, 3224	4732, 4759	6634, 6637	3518, 3545
$m_{\tilde{t}_1}, m_{\tilde{t}_2}$	2272, 3323	2755, 3246	2218, 2740	3671, 4346	6190, 6274	2778, 3104
$m_{\tilde{d}_1}, m_{\tilde{d}_2}$	3840, 3844	3726, 3741	3206, 3225	4760, 4767	6634, 6636	3530, 3546
$m_{\tilde{b}_1}, m_{\tilde{b}_2}$	3298, 4096	3218, 3582	2709, 3077	4321, 4873	6230, 6324	3076, 3287
$m_{\tilde{\nu}_e}, m_{\tilde{\nu}_\mu}$	467.9, 470.6	434.4, 442	444.1, 450.8	385.6, 400.1	520.7, 522.4	414.4, 420.3
$m_{\tilde{l}_1}, m_{\tilde{l}_2}$	378.9, 475.7	435.5, 460.7	370, 452.3	392.4, 812.6	522.8, 596.9	422, 482.2
$m_{\tilde{\tau}_1}, m_{\tilde{\tau}_2}$	1512, 1809	502.4, 1608	351.2, 1484	1128, 2228	1937, 2251	551.8, 1418
$\sigma_{\rm SI}$	7.9×10^{-14}	1.28×10^{-12}	2.02×10^{-12}	2.9×10^{-14}	9.56×10^{-13}	2.25×10^{-10}
$\sigma_{\rm SD}$	7.08×10^{-12}	8.25×10^{-9}	1.85×10^{-8}	3.09×10^{-13}	2.57×10^{-10}	3.22×10^{-6}
Ωh^2	0.115	0.117	0.121	0.118	0.115	0.12

TABLE 1: Benchmark points that exemplify our findings. The points are chosen to be consistent with all the applied constraints including the Planck bound on dark matter. The masses are given in GeV and the cross-sections in pb. Point 1 depicts a solution which is in accord with the Planck bound through the slepton-neutralino coannihilation scenario involving the lighter slepton states from the first two families. Point 2 also exemplifies the solutions for the slepton-neutralino coannihilation scenario with two sleptons involved in the coannihilation processes. Point 3 represents a solution for the stau-neutralino coannihilation scenario, and the first two family sleptons are slightly heavier for such solutions. Point 4 depicts the chargino-neutralino coannihilation scenario. Point 5 also exemplifies solutions of the chargino-neutralino coannihilation, but it also provides an example for A-resonance solutions. Point 6 represents solutions that predict a large spin-independent dark matter scattering cross-section, which can be tested in the near future.

to about 450 GeV at the end of Run-3 phase. However, these bounds hold when the slepton is mostly left-handed; the right-handed slepton can still escape from the detection even when they are as light as about 100 GeV (the solutions with SS $\lesssim 10^{-2}$).

Another LHC probe of the muon $g-2$ solutions can arise from the heavy Higgs boson searches. Figure 10 shows the probe and exclusion for such Higgs bosons through their $\tau\tau$ (left) and bb decays. As seen from the left panel, the current analyses can exclude the muon $g-2$ solutions when $m_A \lesssim 2$ TeV, which leads to the exclusion of the A-resonance solutions. However, the other scenarios for DM and muon $g-2$ can lie slightly below the current exclusion curve, and they are expected to be tested during the Run-3 experiments at LHC. On the other hand, the current analyses do not provide very sensitive results through bb decay modes of the Higgs bosons, the A-resonance solutions can be retested through these analyses. However, we do not expect different results than those obtained through $\tau\tau$ decay modes.

In conclusion, a possible solution to the muon $g-2$ discrepancy seems to favor the nonuniversality in the flavors of the matter fields in light of the current sensitivity of the ongoing experiments. However, the flavor nonuniversality in the models we consider is only imposed to split the third family. Even though it is appealing to accommodate the muon $g-2$ solutions, it cannot explain the discrepancy in the experimental measurements of the electron anomalous magnetic moment. The implications for Δa_e in our models can be extracted by $\Delta a_e/\Delta a_\mu = m_e^2/m_\mu^2$ [74]. However, the experimental measurements reveal $\Delta a_e/\Delta a_\mu = (-14)m_e^2/m_\mu^2$ [75]. Even though the factor can be explained through the new physics, especially the sign in Δa_e requires also possible nonuniversalities between the electron and muon, as well (see, for instance, [76]).

4. CONCLUSION AND SUMMARY

We discussed two classes of SUSY GUT models with nonuniversal boundary conditions imposed at $M_{\rm GUT}$, which are dis-

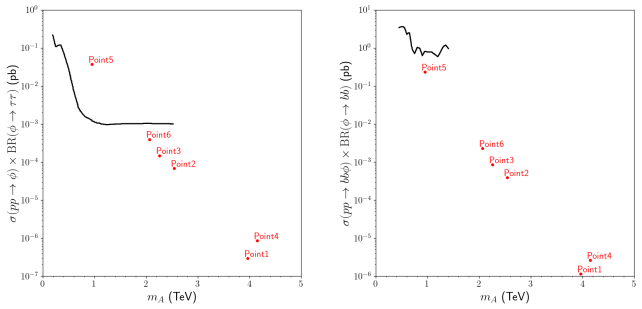

FIGURE 10: The production cross-section times the branching fractions of heavy Higgs boson decays ($\phi \to \tau\tau$ in left, and $\phi \to bb$ in right, where $\phi = H, A$) calculated for the benchmark points listed in Table 1. Each red point corresponds to one benchmark point which is stated above the points. The solid black curve in the left panel represents the exclusion as a function of the CP-odd Higgs boson mass obtained from the analyses in [70, 71]. Similarly, the solid black curve in the right panel is the exclusion obtained from the analyses in [72, 73].

tinguished by the (non)universality of the matter families. We found that the muon $g-2$ solutions can be accommodated even when the models are flavor universal despite the tension with the Higgs boson mass constraint, but the implications of these models are rather challenging to be probed in the current LHC and DM experiments. On the other hand, when the flavor nonuniversal models are considered, the fundamental parameter space is much wider, and the implications can be tested over the chargino-neutralino production processes and heavy Higgs boson decay modes at the LHC experiments. The current analyses can probe the charginos up to about 600 GeV, and these limits can be improved up to about 700 GeV at the end of the Run-3 phase. These bounds hold especially when the sleptons are mostly left-handed. The strongest impact from the current LHC results is observed in A-resonance solutions since the solutions with $m_A \lesssim 2$ TeV are already excluded through $\tau\tau$ decay modes of the heavy Higgs bosons. In addition, the DM phenomenology involves richer implications and they can be expected to be tested in the current and near-future experiments.

CONFLICTS OF INTEREST

The authors declare that there are no conflicts of interest regarding the publication of this paper.

ACKNOWLEDGMENTS

This work is supported in part by the United States Department of Energy grant DE-SC0013880 (Q. Shafi and A. Tiwari). The research of M. Gómez and C. S. Un is supported in part by the Spanish MICINN, under grant PID2019-107844GB-C22. C. S. Un also acknowledges the support in part by the Scientific and Technological Research Council of Turkey (TUBITAK) Grant no. MFAG-118F090. The numerical calculations are performed at the Information Technologies (IT) resources at the University Of Delaware, specifically the high-performance computing resources for the calculation of results presented in this paper.

References

[1] Mario E. Gomez, Qaisar Shafi, Amit Tiwari, and Cem Salih Un. Muon $g-2$, neutralino dark matter and stau NLSP. *Eur. Phys. J. C*, 82(6):561, 2022.
[2] Mario E. Gómez, Qaisar Shafi, and Cem Salih Un. Testing Yukawa Unification at LHC Run-3 and HL-LHC. *JHEP*, 07(07):096, 2020.
[3] Qaisar Shafi and Cem Salih Ün. Sparticle Spectroscopy at LHC-Run3 and LSP Dark Matter in light of Muon $g-2$. 7, 2021.
[4] B. Abi et al. Measurement of the Positive Muon Anomalous Magnetic Moment to 0.46 ppm. *Phys. Rev. Lett.*, 126(14):141801, 2021.
[5] G. W. Bennett et al. Final Report of the Muon E821 Anomalous Magnetic Moment Measurement at BNL. *Phys. Rev.*, D73:072003, 2006.
[6] T. Aoyama et al. The anomalous magnetic moment of the muon in the Standard Model. *Phys. Rept.*, 887:1–166, 2020.
[7] Chih-Ting Lu, Raymundo Ramos, and Yue-Lin Sming Tsai. Shedding light on dark matter with recent muon $g-2$ and Higgs exotic decay measurements. 2021.
[8] Eung Jin Chun and Tanmoy Mondal. Leptophilic bosons and muon $g-2$ at lepton colliders. 2021.
[9] Pritam Das, Mrinal Kumar Das, and Najimuddin Khan. The FIMP-WIMP dark matter and Muon $g-2$ in the extended singlet scalar model. 2021.
[10] M. Cadeddu, N. Cargioli, F. Dordei, C. Giunti, and E. Picciau. Muon and electron $g-2$, proton and cesium weak charges implications on dark Z_d models. 2021.
[11] Juan C. Criado, Abdelhak Djouadi, Niko Koivunen, Kristjan Müürsepp, Martti Raidal, and Hardi Veermäe. Confronting spin-3/2 and other new fermions with the muon $g-2$ measurement. 2021.
[12] Nabarun Chakrabarty. Doubly charged scalars and vector-like leptons confronting the muon $g-2$ anomaly and Higgs vacuum stability. 2020.
[13] Georges Aad et al. Observation of a new particle in the search for the Standard Model Higgs boson with the ATLAS detector at the LHC. *Phys. Lett. B*, 716:1–29, 2012.
[14] Serguei Chatrchyan et al. Observation of a New Boson with Mass Near 125 GeV in pp Collisions at $\sqrt{s} = 7$ and 8 TeV. *JHEP*, 06:081, 2013.
[15] Georges Aad et al. Search for squarks and gluinos in final states with same-sign leptons and jets using 139 fb^{-1} of data collected with the ATLAS detector. *JHEP*, 06:046, 2020.
[16] Tamas Almos Vami. Searches for gluinos and squarks. *PoS*, LHCP2019:168, 2019.
[17] Jovan Mitrevski. Searches for direct pair production of third generation squarks with the ATLAS detector. *PoS*, DIS2018:079, 2018.
[18] Caroline Collard. Searches for third generation squarks with CMS. In *5th Large Hadron Collider Physics Conference*, 9, 2017.
[19] Search for the Supersymmetric Partner of the Top Quark in the Jets+Emiss Final State at $\sqrt{(s)} = 13$ TeV. 8, 2016.
[20] Ali Çiçi, Zerrin Kırca, and Cem Salih Ün. Light Stops and Fine-Tuning in MSSM. *Eur. Phys. J. C*, 78(1):60, 2018.
[21] Zafer Altın, Zerrin Kırca, T. Tanımak, and Cem Salih Ün. Stop search in SUSY $SO(10)$ GUTs with nonuniversal

Gaugino masses. *Eur. Phys. J.*, C80(9):818, 2020.

[22] C. Beskidt, W. de Boer, and D. I. Kazakov. A comparison of the Higgs sectors of the CMSSM and NMSSM for a 126 GeV Higgs boson. *Phys. Lett. B*, 726:758–766, 2013.

[23] C. Strege, G. Bertone, F. Feroz, M. Fornasa, R. Ruiz de Austri, and R. Trotta. Global Fits of the cMSSM and NUHM including the LHC Higgs discovery and new XENON100 constraints. *JCAP*, 04:013, 2013.

[24] John Ellis, Feng Luo, Keith A. Olive, and Pearl Sandick. The Higgs Mass beyond the CMSSM. *Eur. Phys. J. C*, 73(4):2403, 2013.

[25] Ilia Gogoladze, Azar Mustafayev, Qaisar Shafi, and Cem Salih Un. Yukawa Unification and Sparticle Spectroscopy in Gauge Mediation Models. *Phys. Rev. D*, 91(9):096005, 2015.

[26] Yoshiharu Kawamura, Hitoshi Murayama, and Masahiro Yamaguchi. Low-energy effective Lagrangian in unified theories with nonuniversal supersymmetry breaking terms. *Phys. Rev. D*, 51:1337–1352, 1995.

[27] K. S. Babu and Stephen M. Barr. Gauged $SO(3)$ family symmetry and squark mass degeneracy. *Phys. Lett. B*, 387:87–98, 1996.

[28] Mu-Chun Chen and K. T. Mahanthappa. CP violation in a supersymmetric $SO(10) \times U(2)(F)$ model. *Phys. Rev. D*, 65:053010, 2002.

[29] S. F. King and Graham G. Ross. Fermion masses and mixing angles from $SU(3)$ family symmetry and unification. *Phys. Lett. B*, 574:239–252, 2003.

[30] Graham G. Ross, Liliana Velasco-Sevilla, and Oscar Vives. Spontaneous CP violation and nonAbelian family symmetry in SUSY. *Nucl. Phys. B*, 692:50–82, 2004.

[31] K. S. Babu, Ilia Gogoladze, Shabbar Raza, and Qaisar Shafi. Flavor Symmetry Based MSSM (sMSSM): Theoretical Models and Phenomenological Analysis. *Phys. Rev.*, D90(5):056001, 2014.

[32] K. S. Babu, Ilia Gogoladze, Qaisar Shafi, and Cem Salih Ün. Muon $g-2$, 125 GeV Higgs boson, and neutralino dark matter in a flavor symmetry-based MSSM. *Phys. Rev.*, D90(11):116002, 2014.

[33] K. S. Babu, Ilia Gogoladze, and Cem Salih Un. Proton Lifetime in Minimal SUSY $SU(5)$ in Light of LHC Results. 2020.

[34] Ali H. Chamseddine, Richard L. Arnowitt, and Pran Nath. Locally Supersymmetric Grand Unification. *Phys. Rev. Lett.*, 49:970, 1982.

[35] Riccardo Barbieri, S. Ferrara, and Carlos A. Savoy. Gauge Models with Spontaneously Broken Local Supersymmetry. *Phys. Lett. B*, 119:343, 1982.

[36] Nobuyoshi Ohta. GRAND UNIFIED THEORIES BASED ON LOCAL SUPERSYMMETRY. *Prog. Theor. Phys.*, 70:542, 1983.

[37] Lawrence J. Hall, Joseph D. Lykken, and Steven Weinberg. Supergravity as the Messenger of Supersymmetry Breaking. *Phys. Rev. D*, 27:2359–2378, 1983.

[38] Q. Shafi and C. Wetterich. Modification of GUT Predictions in the Presence of Spontaneous Compactification. *Phys. Rev. Lett.*, 52:875, 1984.

[39] B. Ananthanarayan and P. N. Pandita. Sparticle Mass Spectrum in Grand Unified Theories. *Int. J. Mod. Phys.*, A22:3229–3259, 2007.

[40] Subhaditya Bhattacharya, AseshKrishna Datta, and Biswarup Mukhopadhyaya. Non-universal gaugino masses: A Signal-based analysis for the Large Hadron Collider. *JHEP*, 10:080, 2007.

[41] Stephen P. Martin. Non-universal gaugino masses from non-singlet F-terms in non-minimal unified models. *Phys. Rev.*, D79:095019, 2009.

[42] Utpal Chattopadhyay, Debottam Das, and D. P. Roy. Mixed Neutralino Dark Matter in Nonuniversal Gaugino Mass Models. *Phys. Rev.*, D79:095013, 2009.

[43] Achille Corsetti and Pran Nath. Gaugino mass nonuniversality and dark matter in SUGRA, strings and D-brane models. *Phys. Rev.*, D64:125010, 2001.

[44] Kiwoon Choi, Kwang Sik Jeong, and Ken-ichi Okumura. Phenomenology of mixed modulus-anomaly mediation in fluxed string compactifications and brane models. *JHEP*, 09:039, 2005.

[45] Kiwoon Choi and Hans Peter Nilles. The Gaugino code. *JHEP*, 04:006, 2007.

[46] Archana Anandakrishnan and Stuart Raby. Yukawa Unification Predictions with effective "Mirage" Mediation. *Phys. Rev. Lett.*, 111(21):211801, 2013.

[47] Howard Baer, Vernon Barger, Hasan Serce, and Xerxes Tata. Natural generalized mirage mediation. *Phys. Rev. D*, 94(11):115017, 2016.

[48] Shabbar Raza, Qaisar Shafi, and Cem Salih Un. $b-\tau$ Yukawa unification in SUSY $SU(5)$ with mirage mediation: LHC and dark matter implications. *JHEP*, 05:046, 2019.

[49] Jogesh C. Pati and Abdus Salam. Lepton Number as the Fourth Color. *Phys. Rev. D*, 10:275–289, 1974. [Erratum: Phys.Rev.D 11, 703–703 (1975)].

[50] George Lazarides and Q. Shafi. Comments on "Monopole Charges in Unified Gauge Theories". *Nucl. Phys. B*, 189:393, 1981.

[51] T. W. B. Kibble, George Lazarides, and Q. Shafi. Strings in $SO(10)$. *Phys. Lett. B*, 113:237–239, 1982.

[52] K. S. Babu, Borut Bajc, and Shaikh Saad. Yukawa Sector of Minimal $SO(10)$ Unification. *JHEP*, 02:136, 2017.

[53] Takeo Moroi. The Muon anomalous magnetic dipole moment in the minimal supersymmetric standard model. *Phys. Rev.*, D53:6565–6575, 1996. [Erratum: Phys. Rev.D56, 4424 (1997)].

[54] Helvecio Fargnoli, Christoph Gnendiger, Sebastian Paßehr, Dominik Stöckinger, and Hyejung Stöckinger-Kim. Two-loop corrections to the muon magnetic moment from fermion/sfermion loops in the MSSM: detailed results. *JHEP*, 02:070, 2014.

[55] Peter Athron, Markus Bach, Helvecio G. Fargnoli, Christoph Gnendiger, Robert Greifenhagen, Jae-hyeon Park, Sebastian Paßehr, Dominik Stöckinger, Hyejung Stöckinger-Kim, and Alexander Voigt. GM2Calc: Precise MSSM prediction for $(g-2)$ of the muon. *Eur. Phys. J. C*, 76(2):62, 2016.

[56] Felix Brummer, Sabine Kraml, and Suchita Kulkarni. Anatomy of maximal stop mixing in the MSSM. *JHEP*, 08:089, 2012.

[57] Georges Aad et al. Search for electroweak production of charginos and sleptons decaying into final states with two leptons and missing transverse momentum in $\sqrt{s} = 13$ TeV pp collisions using the ATLAS detector. *Eur. Phys. J. C*, 80(2):123, 2020.

[58] Georges Aad et al. Search for direct production of electroweakinos in final states with one lepton, missing trans-

verse momentum and a Higgs boson decaying into two b-jets in pp collisions at $\sqrt{s} = 13\,\text{TeV}$ with the ATLAS detector. *Eur. Phys. J. C*, 80(8):691, 2020.

[59] Search for charginos and neutralinos in final states with two boosted hadronically decaying bosons and missing transverse momentum in pp collisions at $\sqrt{s} = 13\,\text{TeV}$ with the ATLAS detector. 6, 2021.

[60] Morad Aaboud et al. Search for chargino and neutralino production in final states with a Higgs boson and missing transverse momentum at $\sqrt{s} = 13\,\text{TeV}$ with the ATLAS detector. *Phys. Rev. D*, 100(1):012006, 2019.

[61] D. S. Akerib et al. Projected WIMP sensitivity of the LUX-ZEPLIN dark matter experiment. *Phys. Rev.*, D101(5):052002, 2020.

[62] E. Aprile et al. Projected WIMP sensitivity of the XENONnT dark matter experiment. *JCAP*, 2011:031, 2020.

[63] J. Aalbers et al. DARWIN: towards the ultimate dark matter detector. *JCAP*, 1611:017, 2016.

[64] J. Billard, L. Strigari, and E. Figueroa-Feliciano. Implication of neutrino backgrounds on the reach of next generation dark matter direct detection experiments. *Phys. Rev. D*, 89(2):023524, 2014.

[65] Georges Aad et al. Measurement of the $t\bar{t}$ production cross-section in the lepton+jets channel at $\sqrt{s} = 13\,\text{TeV}$ with the ATLAS experiment. *Phys. Lett.*, B810:135797, 2020.

[66] CMS Collaboration. Measurement of the WW cross section pp collisions at $\sqrt{(s)} = 13\,\text{TeV}$. 2016.

[67] Albert M. Sirunyan et al. Measurements of the pp $\rightarrow WZ$ inclusive and differential production cross section and constraints on charged anomalous triple gauge couplings at $\sqrt{s} = 13\,\text{TeV}$. *JHEP*, 04:122, 2019.

[68] Morad Aaboud et al. Measurement of $W^{\pm}Z$ production cross sections and gauge boson polarisation in pp collisions at $\sqrt{s} = 13\,\text{TeV}$ with the ATLAS detector. *Eur. Phys. J.*, C79(6):535, 2019.

[69] Albert M Sirunyan et al. Measurements of the $pp \rightarrow ZZ$ production cross section and the $Z \rightarrow 4\ell$ branching fraction, and constraints on anomalous triple gauge couplings at $\sqrt{s} = 13\,\text{TeV}$. *Eur. Phys. J.*, C78:165, 2018. [Erratum: Eur. Phys. J.C78, no.6, 515 (2018)].

[70] Emanuele Bagnaschi et al. MSSM Higgs Boson Searches at the LHC: Benchmark Scenarios for Run 2 and Beyond. *Eur. Phys. J. C*, 79(7):617, 2019.

[71] Georges Aad et al. Search for heavy Higgs bosons decaying into two tau leptons with the ATLAS detector using pp collisions at $\sqrt{s} = 13\,\text{TeV}$. *Phys. Rev. Lett.*, 125(5):051801, 2020.

[72] Georges Aad et al. Search for heavy neutral Higgs bosons produced in association with b-quarks and decaying into b-quarks at $\sqrt{s} = 13\,\text{TeV}$ with the ATLAS detector. *Phys. Rev. D*, 102(3):032004, 2020.

[73] Albert M Sirunyan et al. Search for a charged Higgs boson decaying into top and bottom quarks in events with electrons or muons in proton-proton collisions at $\sqrt{s} = 13\,\text{TeV}$. *JHEP*, 01:096, 2020.

[74] Marcin Badziak and Kazuki Sakurai. Explanation of electron and muon $g-2$ anomalies in the MSSM. *JHEP*, 10:024, 2019.

[75] Richard H. Parker, Chenghui Yu, Weicheng Zhong, Brian Estey, and Holger Müller. Measurement of the fine-structure constant as a test of the Standard Model. *Science*, 360:191, 2018.

[76] Mariana Frank, Yaşar Hiçyılmaz, Subhadeep Mondal, Özer Özdal, and Cem Salih Ün. Electron and muon magnetic moments and implications for dark matter and model characterisation in non-universal $U(1)'$ supersymmetric models. *JHEP*, 10:063, 2021.